



# CHORUS

This is the accepted manuscript made available via CHORUS. The article has been published as:

## Detection of (2,2) quasinormal mode from a population of black holes with a constructive summation method

C. F. Da Silva Costa, S. Tiwari, S. Klimenko, and F. Salemi

Phys. Rev. D **98**, 024052 — Published 31 July 2018

DOI: [10.1103/PhysRevD.98.024052](https://doi.org/10.1103/PhysRevD.98.024052)

# Detection of (2,2) quasi normal mode from a population of black holes with a constructive summation method

C. F. Da Silva Costa<sup>1</sup>, S. Tiwari<sup>2,3</sup>, S. Klimentko<sup>1</sup>, F. Salemi<sup>4</sup>

(1) *University of Florida, Gainesville, Florida, USA* \*

(2) *INFN, Trento Institute for Fundamental Physics and Applications, Trento, Italy*

(3) *Gran Sasso Science Institute (INFN), Via F. Crispi 7, I-67100, L'Aquila, Italy and*

(4) *Albert-Einstein-Institut, Max-Planck-Institut für Gravitationsphysik, Hannover, Germany*

(Dated: May 19, 2018)

The quasi normal modes (QNMs) associated with gravitational-wave signals from binary black hole (BBH) mergers can provide deep insight into the remnant's properties. Once design sensitivity is achieved, present ground-based gravitational wave interferometers could detect potentially hundreds of BBH signals in the coming years. But for most, the ringdown phase will have a very weak signal-to-noise ratio (SNR) and therefore poor, if any, scientific information could be extracted from them. We review how a summation method can help detect these weak (2,2) QNMs and potentially allow to use their information. The method is based on two main steps: signal's rescaling and synchronization. In this first study, we tested the method under limited BBH parameters and review its principal limitations. In particular, the synchronization which fails for the weakest signals, requires selecting ringdowns with SNR above 2.6. Using this threshold, we show that for two different BBH populations, 40 to 70% of all the potential detections could still be used for the summation while ensuring a summed SNR of  $\sim 80\%$  of the maximal achievable SNR (i.e. for ideally synchronized signals).

## I. INTRODUCTION

A binary black hole (BBH) is expected to form a perturbed Kerr black hole (BH) [1]. Its perturbations are damped oscillations [2], which are the superposition of quasi normal modes (QNMs) [3, 4]. According to the no-hair theorem [5], a Kerr black hole can be described by two parameters, its mass,  $M_{BH}$ , and its dimensionless spin,  $a$ , see Section II. If these two BH parameters could be measured, then they can be used to carry out tests of general relativity [6, 7].

Presently, the rate of stellar mass BBH mergers is estimated to be  $12\text{--}213 \text{ Gpc}^{-3}\text{yr}^{-1}$  [8]; implying the possible detection of hundreds of BBHs in the coming years by GW interferometers [9]. Most of these BBH signals are expected to have a weak ringdown where no information can be extracted. Indeed, considering the four LIGO observed BBH merger events: GW150914, GW151226, GW170104 and GW170814 [8, 10–12], only GW150914 has a ringdown with a high enough signal-to-noise ratio (SNR  $\sim 7$ ) to extract information [7, 13–15].

For this reason, methods being developed to detect QNMs from BHs [16–20] are targeting the more sensitive future generations of ground and space-based detectors. High SNR ringdown signals will be most likely rare, allowing informative general relativity consistency tests in only a few cases. However, signal summation techniques [18, 21] applied to most weak ringdown signals can help to extract information otherwise lost.

We tested a method, see Section III, to constructively sum up the dominant (2,2) QNM from several BBH

signals. To be summed constructively the signals are rescaled and synchronized. The resultant signal is a “normalized” (2,2) mode which could be used to infer the properties for the population of remnant BHs, i.e. “normalized” mass,  $M'_{BH}$ , and spin,  $a'$ . This, in turn, can provide a weak test on the Kerr nature of the BH population. The subdominant modes  $lm=(3,3)$ , (2,1) and (4,4) could provide tighter constraints on the BH population's Kerr nature, but presently there is no solution to synchronize the subdominant modes at the same time as the (2,2) modes.

In this paper we do not explore the Kerr tests, but if the QNM signals could be extracted with a substantial SNR that allows the normalized parameters to be measured. In Section IV, we report the results of tests done with two populations of simulated ringdowns. Finally in Section V, we summarize the results and the present limitations under which the method was tested, and discuss potential improvements to the method.

## II. QUASI NORMAL MODES GRAVITATIONAL WAVES

The QNM gravitational waves are given by:

$$h = \sum_{nlm} {}_{-2}Y_{lm}(\iota, \phi) h_{nlm}, \quad (1)$$

where  ${}_{-2}Y_{lm}$  are the spin-weighted spherical harmonics. The index  $n$  is the overtone and in what follows we will consider only  $n = 0$  to be the strongest modes.  $l, m > 0$  are the spheroidal harmonic indices. The angles are given in the source frame:  $\iota$  is the angle between the system spin and the line of sight, and  $\phi$  is the azimuth angle. The GW amplitudes of the QNMs are defined by:

\* filipe.dasilva@ufl.edu

$$h_{lm} = A_{lm} \frac{M_{BH}}{r} e^{-\pi f_{lm}/Q_{lm}t} \sin(2\pi f_{lm}t + \Phi_{lm}), \quad (2)$$

where  $A_{lm}$  and  $\Phi_{lm}$  are the amplitude and phase of each mode respectively. They depend on physical phenomena happening inside the BH and will be provided by simulations.  $M_{BH}$  is the remnant BH's mass, and  $r$  is the distance to the source. Frequencies,  $f_{lm}$ , and quality factors,  $Q_{lm}$ , are related to the remnant black hole mass,  $M_{BH}$ , and the dimensionless spin,  $a$ , [19, 22]:

$$f_{lm} = \frac{1}{2\pi} \frac{c^3}{GM_{BH}} [f_1 + f_2(1-a)^{f_3}] \quad (3)$$

$$Q_{lm} = q_1 + q_2(1-a)^{q_3}. \quad (4)$$

where  $a = [0, 1]$ ;  $a = 0$  implies non-spinning while  $a = 1$  corresponds to the maximum spin, where the innermost stable circular orbit is close to the BH radius.

### III. METHOD DESCRIPTION AND TEST LIMITATIONS

In order to constructively sum all the (2,2) modes, the ringdown signals are rescaled so that they have the same  $f_{22}$  frequency, and then they are synchronized to a common time reference. Prior information for these two steps is needed: (2,2) frequencies, peak times, and mass ratios. They could be estimated by *LALInference* using the inspiral-merger part of the signal [23]. In this first study we do not consider error propagation from other methods.

We tested these two steps with and without noise. The subdominant modes change the GW signals, so we take them into account to understand their effect on the signal's synchronization and on the measurements of the normalized parameters. For these reasons, we used numerical relativity waveforms from SXS [24–29] that allow us to have all the mode information without noise, see Fig. 1. Then we inject these waveforms into Gaussian noise. In Section III, we do not take into account the detector PSD for simplification. It would introduce errors that are not related to the method used here, and when we will band-pass filter the signal around the (2,2) mode frequency, the noise could as good approximation be considered as Gaussian. Instead, in section IV, for the general BBH population study, it is taken into account. But in both Sections we will give our results in terms of SRN to remain independent of detector PSD's. After the summation the SNR and the normalized parameters of the resulting signal are measured.

We define two SNRs: the SNR of the QNMs,  $\text{SNR}_{QNM}$ , which is defined from the ringdown's synchronization points, and the ringdown SNR,  $\text{SNR}_{RD}$ , which is defined from the peak amplitude, see Fig. 1, plot “ $q = 1.5$ ”.  $\text{SNR}_{RD}$  will be used to select the ringdown

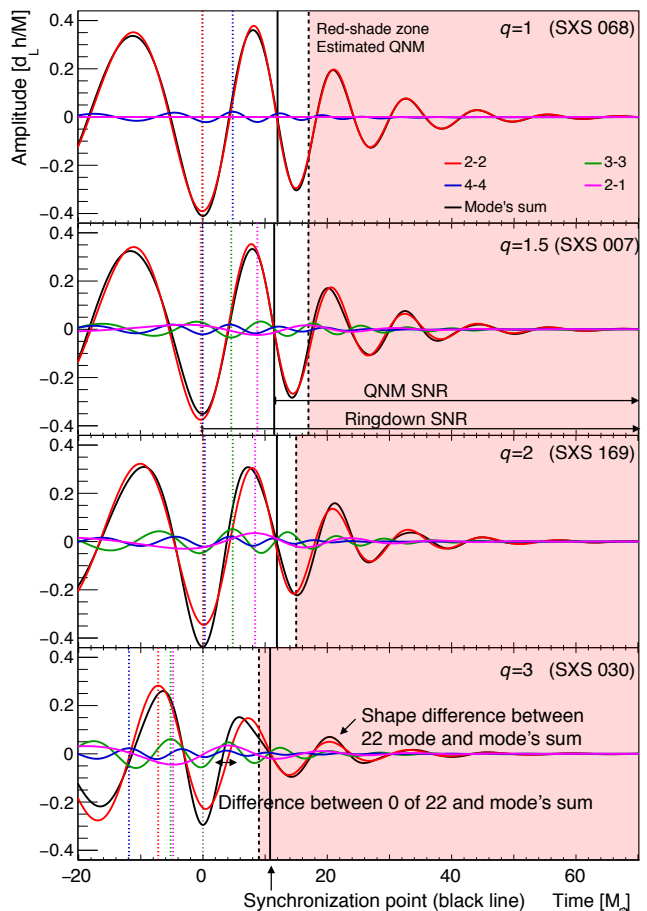


Figure 1. BBH SXS waveforms chosen for our tests:  $q \leq 3$ , non-spinning initial BHs with face-on orientation. The QNMs are: red=(2,2), green=(3,3), blue=(4,4), pink=(2,1) with black representing the QNM sum. We set  $t = 0$  at the signal maximum amplitude. Short dashed lines mark the maximum of their corresponding mode. The red-shaded zone mark the estimated region of QNMs. The vertical solid black lines indicate the point from which we synchronize the ringdown signals.

signals as it includes a visible part of the signal, while  $\text{SNR}_{QNM}$  is the SNR of the signals being accumulated.

The method efficiency is measured using the “summation efficiency” ( $\text{SUM}_{eff}$ ) defined as the ratio between the measured  $\text{SNR}_{QNM}$  and the maximum expected  $\text{SNR}_{QNM}$  of the summed signals:  $\text{SUM}_{eff} = \text{SNR}_{QNM \text{ measured}} / \text{SNR}_{QNM \text{ expected}}$ . The maximum cumulated  $\text{SNR}_{QNM}$  is achieved when all signals are perfectly synchronized, which is given by:

$$\text{SNR}_{QNM \text{ expected}} = \left( \sum_{i=1}^N \text{SNR}_{QNM i}^2 \right)^{1/2}, \quad (5)$$

where  $\text{SNR}_{QNM i}$  is the SNR of each signal and  $N$  is the total number of signals.

The normalized spin and mass of the resulting signal are extracted by fitting it with Eq. 2 applied to the (2,2) mode:

$$h_{22} = A_{22}e^{-\pi f_{22}/Q_{22}t} \cos(2\pi f_{22}t + \Phi_{22}). \quad (6)$$

All constants are included in the amplitude  $A_{22}$ . For the (2,2) mode, Eqs. 3 and 4 are given by:

$$f_{22} = \frac{1}{2\pi M_{BH}} [1.525 - 1.157(1 - a)^{0.129}], \quad (7)$$

$$Q_{22} = 0.700 + 1.419(1 - a)^{-0.499}. \quad (8)$$

The speed of light in the vacuum and the gravitational constant are set,  $c = G = 1$ , to match the SXS waveform units.

The expected value of the normalized mass  $M'_{BH}$ , and spin,  $a'$ , could be estimated by summing the  $N$  hypothetical signals we have in our data:

$$h'_{22} = \sum_{i=1}^N A_{22i} e^{-\pi f_{22i}/Q_{22i}t} \cos(2\pi f_{22i}t + \Phi_{22i}). \quad (9)$$

These estimations, as we recall, comes from the inspiral-merger part. After the rescaling all the frequencies are the same  $f_{22i} = f'_{22}$ . The synchronization aligns all phases, then we can set to  $\Phi_{22i} = 0$ . Therefore, Eq. 9 rewrites:

$$h'_{22} = \cos(2\pi f'_{22}t) \sum_{i=1}^N A_{22i} e^{-\pi f'_{22}/Q_{22i}t}, \quad (10)$$

thus the new damping factor  $Q'_{22}$  could be determined by:

$$A'_{22} e^{-\pi f'_{22}/Q'_{22}t} = \sum_{i=1}^N A_{22i} e^{-\pi f'_{22}/Q_{22i}t}. \quad (11)$$

We adopted another approach, as data analysts, we sum the numerical waveforms without noise and fit the resultant signal to extract mass  $M'_{BH}$ , and spin  $a'$ .

QNMs are dependent on many parameters which have different impact on the method that should be studied. But our first objective is to understand how well we can extract the (2,2) modes from the noise and we focus on the synchronisation. Therefore we choose to primarily test the present method with a reduced set of parameters. First, we consider only the strongest modes  $n = 0$  as already mentioned and  $(l, m) = (2, 2), (3, 3), (4, 4)$  and  $(2, 1)$ . The present detections have a mass ratio,  $q$ , between 1 and 2 therefore we constrain  $q \leq 3$  and we will consider the exact mass ratio without error propagation from the other methods. We also limit our study to initially spinless BBHs and used an average orientation over the sky. Given these constrains, between the SXS waveforms we choose the following ones shown Fig. 1 and detailed in Appendix 2.

## A. Rescaling

The rescaling is achieved by resampling the signals according to the  $f_{22}$  ratio:

$$sample(q) = f_{22}(q)/f_{22}(q=1) sample(q=1). \quad (12)$$

For the current study, we derived a fitting function for spinless BHs, by using the SXS metadata, this gives the  $f_{22}$  ratio:

$$\frac{f_{22}(q)}{f_{22}(q=1)} = 0.0032q^2 - 0.0583q + 1.0604. \quad (13)$$

As shown in Tab. I, the periods of the four ringdowns are consistent with one another, showing that the rescaling procedure does not introduce large errors by itself.

Table I. Average waveforms periods  $\langle T \rangle$  after rescaling in the QNM linear regime.

Mass ratio $q$	Average period $\langle T \rangle$ [ $M_{\odot}$ ]	$\langle \langle T \rangle \rangle_q = 11.55$ $\sigma(\langle T \rangle)_q = 0.20$
1	11.51	
1.5	11.37	
2	11.53	
3	11.84	

## B. Synchronization

As indicated in [30], after the peak GW luminosity, effects of the merging phase are still present in the ringdown. The authors identified the beginning of the QNMs with the stabilization in time of the remnant BH frequencies. We proceed with similar tests to estimate the QNM starting time. We fit the ringdown waveforms (without noise) at different times using the (2,2) function, Eq. 6, and we define the QNM starting time when the spin  $a$  becomes constant. The starting times are shown in Fig. 1 and are compatible with those in [30].

As shown in Fig. 1, the QNMs start approximatively one period after the maximum amplitude. Though any time after one period can be chosen for synchronization, “later” times are disadvantageous due to the quick dampening of QNMs; it is difficult to identify a synchronization point after only one oscillation, while the lower SNR requires more events to extract information.

Therefor as a compromise between the low SNR and the influence by the non-linear merger effects, we choose the second zero after the peak amplitude as the synchronization point, see Fig. 1. The error due to the merger effect are compared at 3 different times and shown in Tab. II.

In the QNM regime, we observe systematic errors:  $\sim 10\%$  higher for the spin  $a$  and  $\sim 5\%$  for the mass,  $M_{BH}$ , with respect to the SXS metadata. Part of the

Table II. Relative error on the mass,  $M_{BH}$ , and spin,  $a$ , with respect to SXS metadata at 3 different times: the maximum amplitude ( $t=0$ ), the synchronization point and the estimated beginning of the QNM. The signal is fitted with the (2,2) mode function, Eq. 6.

Mass ratio $q$	Relative errors [%]					
	$t = 0$		Synchronisation point		QNM regime	
	$a$	$M_{BH}$	$a$	$M_{BH}$	$a$	$M_{BH}$
1	42	42	30	9	15	6
1.5	44	40	14	7	12	5
2	47	36	13	6	15	5
3	30	12	6	1	10	3

errors in Tab. II are also due to the difference between the (2,2) mode, which serves as a fitting function, and the actual GW signal, which is the sum of all the modes, see Fig. 1,  $q = 3$ . These errors are expected to be reduced by the summation.

The synchronization point (2nd zero of waveform after the maximum) is determined by fitting a sine-exponential function, covering a half period, around its expected time, which, in turn, is estimated by using our knowledge on the maximum amplitude time and expected frequency of the signal. The fit is improved by setting its initial parameters, the frequency and damping coefficients, to the values estimated for the rescaling process. The signal is further improved by band-passing it with a narrow window around the mode frequencies. The error shift between the (2,2) mode zero and the fitted zero are shown in Fig. 2. When the  $\text{SNR}_{RD} \leq 1$ , the synchronization errors are constrained by the implemented limits of the fit.

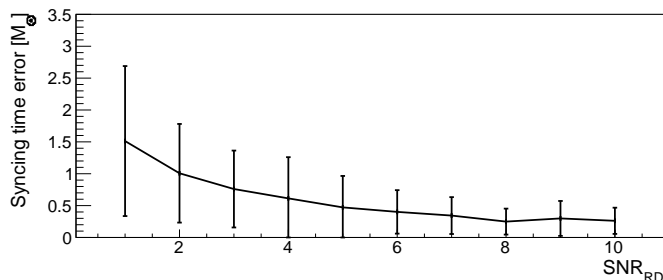


Figure 2. Average time shift errors between the (2,2) mode zero and the fitted waveform zero: For each mass ratio and SNR level, the average is computed with 50 injections of the waveforms including the four modes (2,2), (3,3), (4,4) and (2,1). Error bars represent standard deviations.

### C. Subdominant mode perturbations

The subdominant modes are rescaled simultaneously with the (2,2) mode due to the constant ratios between mode frequencies  $f_{22}/f_{lm}$ . However, they are not synchronized when synchronizing the (2,2) modes as the phase differences between the (2,2) modes and the subdominant modes are different for each  $q$ . In these conditions, the divergence introduced by the summed subdominant modes to the (2,2) mode fit cannot be modeled. The subdominant modes are therefore considered as perturbative noise.

The BBH inclination changes the relative amplitude between the modes as shown by Eqs 20-23 in [30]. The highest mode contribution, for the self-imposed upper limit  $q = 3$ , comes from the subdominant mode (2,1) of an edge-on system which reach up to  $\sim 0.6$  times the (2,2) mode amplitude. The contribution of (2,1) mode is still low as compared to the (2,2) mode for the mass ratios considered. But as the subdominant modes are not summed constructively, the amplitude ratios of the summed signals are lower than for a single signal. In Fig. 3, we show a comparison of the amplitude ratios  $A_{33}/A_{22}$ ,  $A_{21}/A_{22}$  and  $A_{44}/A_{22}$  of single signals with the amplitude ratios of summed signals. In both cases we used an averaged orientation. The highest contribution is  $A_{33}/A_{22} = 0.23$  [30] and drops to  $A_{33}/A_{22} < 0.1$ . This allows us, for now, to neglect their effect in the summation.

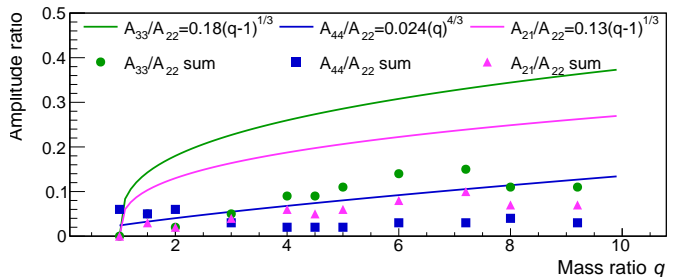


Figure 3. Amplitude ratios between the (2,2) mode and subdominant orders  $A_{33}/A_{22}$ ,  $A_{21}/A_{22}$  and  $A_{44}/A_{22}$  for different mass ratio  $q$ . Continuous lines represent amplitude ratio functions previously derived ( $t=10 M_{\odot}$  after the (2,2) peak) [30] for single signals. The markers represent the maximum mode ratios when summing all signals from  $q = 1$  till the indicated  $q$ . For instance at  $q = 3$ ,  $q=1, 1.5, 2$  and  $3$  are summed.

In the case of single signals, the subdominant mode affect the synchronization point, changing its time. Their effect is proportional to the subdominant modes' amplitudes, thus increasing with  $q$  as shown in Fig. 1. The largest synchronization shift,  $t_s$ , is achieved when they are in phase with each other but not with the (2,2) mode maximum. In this scenario, the synchronization points shift between the (2,2) mode zero and the ringdown zero by  $t_s = \{0.4, 0.8, 0.9, 1.5\} M_{\odot}$

for  $q = \{1, 1.5, 2, 3\}$ . The error introduced is comparable to the time shift due to noise at  $\text{SNR} = 4$ , see Fig. 2.

#### D. Cumulated SNR and parameter extraction

Once we rescaled and synchronized the signals, we tested how the  $\text{SNR}_{QNM}$  improved with the summation, and which resolution can be achieved on the normalized parameters. We proceed to inject our four SXS signals into white noise with 10 different  $\text{SNR}_{QNM}$  and then for each  $\text{SNR}_{QNM}$ , we sum up, incrementally, 20 randomly sampled signals. It does means we re-used the same waveforms (same  $q$ ) multiple times in different noise. We keep the average orientation which imply the average ratio between mode amplitudes.

The cumulated SNR, according to Eq. 5, should increase by a factor  $\sqrt{N}$ . In Fig. 4 is shown the  $\text{SNR}_{QNM}$  of the resulting signal from the summation. For low  $\text{SNR}_{RD}$ , the synchronization errors are higher, see Fig. 2, therefore the signals are not summed constructively, and the ratios shown in the low  $\text{SNR}_{QNM}$  columns are lower than  $\sqrt{N}$ .

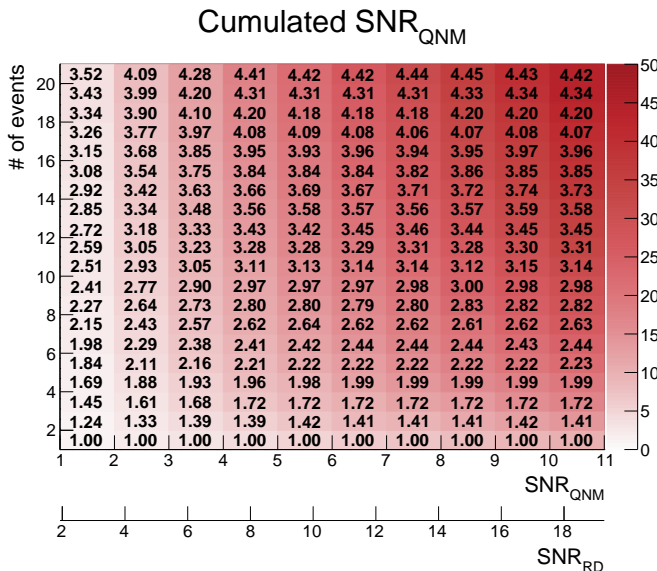


Figure 4. Cumulated  $\text{SNR}_{QNM}$  from  $N$  event signals with the same original  $\text{SNR}_{QNM}$ : For each entry of the table, the test is repeated 50 times with waveforms chosen randomly between the 4 mass ratios. The color scale indicates the average cumulated  $\text{SNR}_{QNM}$  and the written numbers correspond to the ratio between injected and the averaged cumulated  $\text{SNR}_{QNM}$ . The  $\text{SNR}_{RD}$  scale is shown for indication about the SNR being used for synchronization.  $\text{SNR}_{QNM}$  indicates that the QNM are not visible but the first oscillation from the maximum amplitude is visible.

The expected spin and mass values of the resulting signal from the four randomly sampled waveforms

with the same  $\text{SNR}_{QNM}$  are inferred by fitting the signal sum without noise. The fit results are  $a' = 0.66$  and  $M'_{BH} = 1.0 [M_{BH}/M_{BBH}]$  (The SXS remnant mass is given proportionally to the BBH initial total mass). These values are affected by the aforementioned errors in the previous section (e.g. propagation of non-linear mergers effects in the ringdown and, discrepancy between the (2,2) mode and the actual GW signal) which explains why  $M_{BH} \not\prec 1$ . The average and standard deviations of

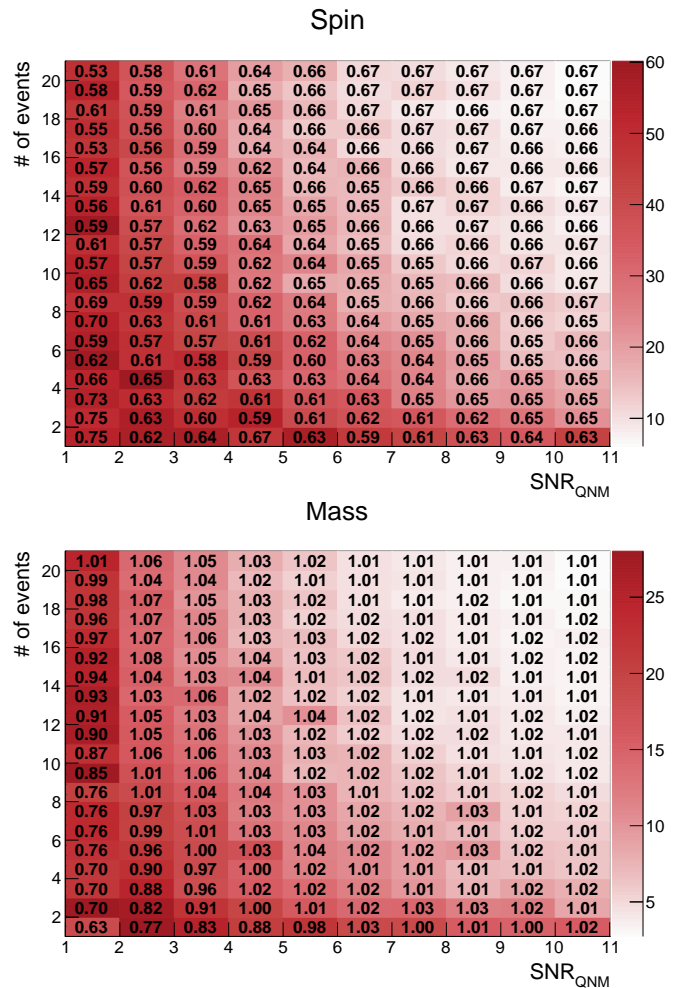


Figure 5. Average and standard deviations of the fitted spin and mass values from  $N$  event signals with the same original  $\text{SNR}_{QNM}$ : The color scale indicates the standard deviation in % while the written numbers correspond to the average (each test is repeated 50 times). The waveforms are chosen randomly between the 4 mass ratios and the resultant signal is fitted with the (2,2) mode functions Eqs. 7-8.

the fitted spin and mass values from  $N$  event (normalized values) as a function of the  $\text{SNR}_{QNM}$  and the number of summed signals are shown in Fig. 5. With a collection of low  $\text{SNR}_{QNM}$  signals, the standard deviation is up to 60% on the spin and is 30% on the mass. This, however, improves for the higher  $\text{SNR}_{QNM}$ , e.g. for 10 signals with  $\text{SNR}_{QNM} = 3$ , precisions on the spin and mass are

respectively 35% and 15%. Except for small variations, the precision follows this cumulated  $\text{SNR}_{QNM}$  trend. For values of signals with  $\text{SNR} \geq 10$ , the precision is compatible with the ones predicted in [31].

#### IV. APPLICATION TO A POPULATION OF SIMULATED RINGDOWNS

The main interest of the summation method is to retrieve physical information from signals of weak  $\text{SNR}_{RD}$ , that would not have been used otherwise. In order to understand how many events could be employed in our analysis, we simulate, using SEOBNR [32], the  $\text{SNR}_{RD}$  distributions from merger signals of two BBH populations of different mass distributions: *uniform* distribution in component masses and *flat* in  $\log(m_1)$  and  $\log(m_2)$ , see Fig. 6. The SNRs are given for the designed sensitivity of the advanced interferometers LIGO and VIRGO [33]. Only events with total  $\text{SNR} > 8$  (complete signal) are selected. Each population has 1000 events. The BBHs are uniformly distributed in volume and with a total mass between 10-100  $M_\odot$ . Then, for each population the 4 waveforms are randomly sampled and injected into noise with a random value  $\text{SNR}_{RD}$  from the distributions and the summation is applied.

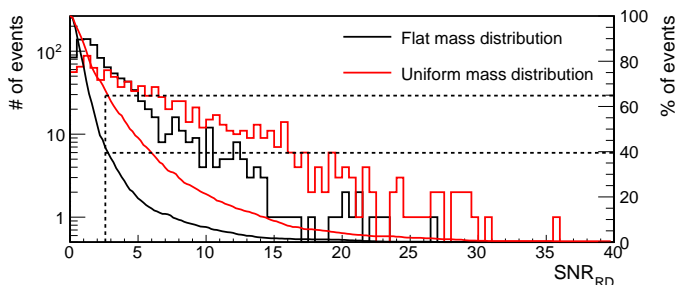


Figure 6. The histograms represent the number of events with the respective  $\text{SNR}_{RD}$  for each BBH mass distribution (black for flat and red for uniform). The receiver operating characteristic (ROC) for the two mass distributions is represented by the solid lines (number of events against  $\text{SNR}_{RD}$ ) while the  $\text{SNR}_{RD}$  threshold is highlighted with the dashed line.

As we have seen in Section III B, the synchronization errors, which prevent the signals from being summed constructively, are worse for lower  $\text{SNR}_{RD}$ . It is therefore beneficial to introduce a  $\text{SNR}_{RD}$  threshold, which will allow us to select those events with usable  $\text{SNR}_{RD}$ . In Fig. 7, the  $\text{SUM}_{eff}$  as a function of different  $\text{SNR}_{RD}$  thresholds is shown (remember, for the synchronization we use  $\text{SNR}_{RD}$  but the efficiency is computed with  $\text{SNR}_{QNM}$ ). The results for 3  $\text{SNR}_{RD}$  distributions (the two mass distribution and a limit case with  $\text{SNR}_{RD}$  equal to the threshold) are compared with 80% efficiency; this value was chosen as the curves stabilize above it. The

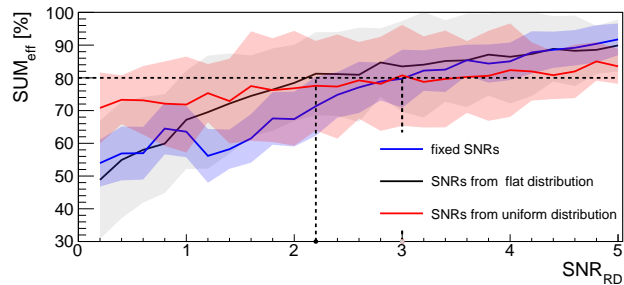


Figure 7. Summation efficiency,  $\text{SUM}_{eff}$ , as a function of different  $\text{SNR}_{RD}$  thresholds for 3  $\text{SNR}_{RD}$  distributions. The blue line corresponds to simulations with SNRs equal to the threshold, i.e. fixed. The red and black lines are the SNRs of the uniform and flat populations respectively. For each entry, 20 event signals are summed and the test is repeated 20 times; the color bands represent the standard deviations.

flat mass distribution has the highest  $\text{SNR}_{RD}$  from its detected signals and its curve passed 80% efficiency at a lower threshold,  $\text{SNR}_{RD} = 2.2$ , than the other distributions; their curves reach 80% efficiency at  $\text{SNR}_{RD} = 3$ . These efficiency values lie between a non-constructive summation of 20 signals, 47% ( $N^{-1/4}$ ), and fully constructive, 100%. At very low  $\text{SNR}_{RD}$  ( $\sim 0.2$ ) the efficiency should be lower than the shown  $\sim 50\%$ . This is due to a method artefact; the fit covers a region where the signal's zero is expected, thus all synchronization times are close to the real ones.

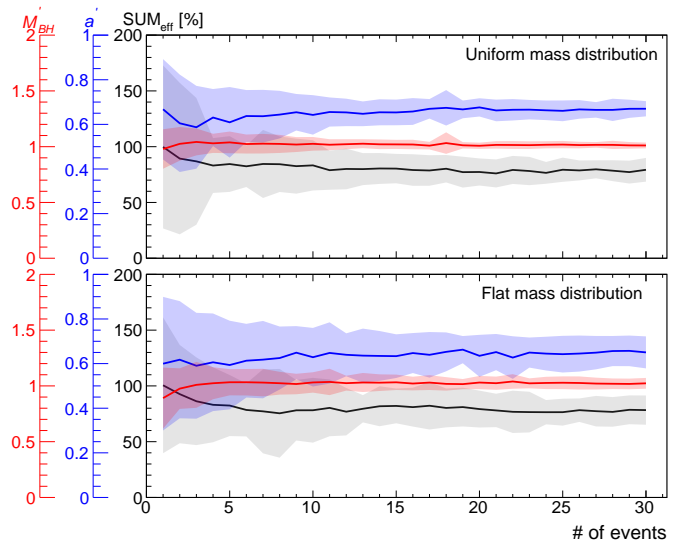


Figure 8. Average values of mass, spin and  $\text{SUM}_{eff}$  for different numbers of event signals summed. The expected values are:  $M'_{BH} = 1$ ,  $a' = 0.66$ , and  $\text{SUM}_{eff} = 80\%$ . The average is computed with 20 repetitions, and the color bands represent the standard deviations.

Taking into account standard deviations of the 3 curves

around 80% efficiency, we choose a threshold  $\text{SNR}_{RD} \geq 2.6$ . Depending on the expected BBH mass distribution, 40% to 70% of the signals will be selected, see Fig. 6. In Fig. 7, the  $\text{SUM}_{eff}$  is computed for 20 summed signals. In Fig. 8, the  $\text{SUM}_{eff}$ , the mass and the spin are shown for several numbers of summed signals after applying the chosen threshold,  $\text{SNR}_{RD} = 2.6$ . The average of the  $\text{SUM}_{eff}$  stabilizes around 80% as expected. The standard deviation for a few events is large because it depends directly on the  $\text{SNR}_{RD}$  distributions; while for more events, this effect is averaged. In addition, the standard deviations of the flat mass distribution are still larger due to its bulkier distribution at low  $\text{SNR}_{RD}$ . The precision of the mass and spin in both cases follow the SNR trend.

## V. CONCLUSION

We tested the signal summation method that we developed for the (2,2) mode. For simplification we reduced the parameter space of the used BBH. These results showed that the synchronization is a critical point for a constructive summation. Other parameters like for example the mass ratio error propagation from the inspiral-merger will also affect the summation but in a different way. In this case it changes the frequency rescaling and it will also introduce errors to the normalized parameters but, this is out of the present scope. Thus considering mainly synchronization problems, we showed that the summation method, after selecting signals with  $\text{SNR}_{RD} \geq 2.6$ , can ensure a signal summation efficiency of 80%. Depending on the expected BBH mass distribution, 40 to 70% of the potential BBH signals detected can still be used to extract normalized remnant properties.

We are presently working to include more parameters in our tests. To consider spinning initial BHs, we have to adopt the three dimensional function: spin and mass ratio vs (2,2) frequencies, for instance derived in [34]. The effects of the subdominant modes were averaged by using an averaged sky direction, we will introduce different BH orientations. And as we mentioned, the error propagation on the mass ratio inferred from the inspiral-merger will be incorporated in future results. All these points will not affect the numbers of BBH system we can use as they depend mainly on the individual SNRs but will affect the summation efficiency and consequently the normalized parameters. This will require an independent study of the extractable information.

We are also working on new and more robust signal synchronization techniques to allow the use of more signals. Finally, an important step will be the synchronization of the subdominant modes. Their information will

allow a more constraining test on the Kerr nature of the remnant BH population.

## ACKNOWLEDGMENTS

This work has been supported by NSF grant PHY 1505308. S. Tiwari is supported by the People Program (Marie Curie Actions) of the European Union FP7/2007-2013/ (PEOPLE-2013-ITN) under REA grant agreement No. [606176].

We would like to acknowledge with much appreciation the discussions with A. Heffernan, B. F. Whiting and L. London. We acknowledge the comments and references that C. Lousto gave us. We also thank the SXS collaboration, M. Boyle and H. Pfeiffer, for kindly answering our questions. For their support L. Da Silva and A. Dusty.

## APPENDIX

### 1. QNM fitting functions

Several authors [22, 35–37] have developed semi-analytic or numerical methods to compute the QNMs. Nowadays, the parameters  $f_1, f_2, f_3, q_1, q_2$  and  $q_3$  are determined by fitting simulation results [19, 38], the modes  $(l, m) = (2, 2), (3, 3), (2, 1)$  and  $(4, 4)$  are then given by:

$$f_{22} = \frac{1}{2\pi} \frac{c^3}{GM_{BH}} [1.525 - 1.157(1-a)^{0.129}] \quad (14)$$

$$Q_{22} = 0.700 + 1.419(1-a)^{-0.499} \quad (15)$$

$$f_{21} = \frac{1}{2\pi} \frac{c^3}{GM_{BH}} [0.600 - 0.234(1-a)^{0.418}] \quad (16)$$

$$Q_{21} = -0.300 + 2.356(1-a)^{-0.228} \quad (17)$$

$$f_{33} = \frac{1}{2\pi} \frac{c^3}{GM_{BH}} [1.896 - 1.304(1-a)^{0.182}] \quad (18)$$

$$Q_{33} = 0.900 + 2.343(1-a)^{-0.481} \quad (19)$$

$$f_{44} = \frac{1}{2\pi} \frac{c^3}{GM_{BH}} [2.300 - 1.505(1-a)^{0.224}] \quad (20)$$

$$Q_{44} = 0.700 + 1.419(1-a)^{-0.483} \quad (21)$$

### 2. Tested waveforms

All the SXS waveforms used for our tests are listed in Tab. III; they are low eccentricity and non-spinning initial BHs. For the ringdown, we use a specific set of data called “outermost”, where NR extractions were performed without extrapolation. This set better describes the ringdown as extrapolations will contain numerical errors.

Table III. Chosen simulations from SXS. All values are expressed in geometrical units,  $c = G = 1$ , the time is normalized by the total initial mass  $M_{BBH}$  while the initial masses are normalized to  $M_{BBH} = 1$ .

Mass ratio $q$	Waveform Id.	Mass $M_{BH}$	Spin $a$
1	002	0.952	0.622
1.5	007	0.955	0.606
2	169	0.961	0.576
3	030	0.971	0.510
4	167	0.978	0.451
4.499	190	0.980	0.425
5	054	0.982	0.402
6	166	0.985	0.362
7.187	188	0.988	0.323
8	063	0.989	0.300
9.167	189	0.990	0.273

- 
- [1] R. P. Kerr, Phys. Rev. Lett. **11** (1963).  
[2] C. V. Vishveshwara, Phys. Rev. D **1** (1970).  
[3] W. H. Press, The Astrophysical Journal **170**, L105 (1971).  
[4] H.-P. Nollert, Classical and Quantum Gravity **16**, R159 (1999).  
[5] R. Ruffini and J. Wheeler, Physics Today (1971).  
[6] S. Gossan, J. Veitch, and B. S. Sathyaprakash, Physical Review D **85** (2012).  
[7] A. Ghosh, N. K. Johnson-McDaniel, A. Ghosh, C. K. Mishra, P. Ajith, W. D. Pozzo, C. P. L. Berry, A. B. Nielsen, and L. London, arXiv:1704.06784 (2017).  
[8] B. P. Abbott *et al.* (LIGO Scientific Collaboration, Virgo Collaboration), Phys. Rev. Lett. **118** (2017).  
[9] J. Abadie *et al.*, Class. Quantum Grav. **27** (2010).  
[10] B. P. Abbott *et al.* (LIGO Scientific Collaboration, Virgo Collaboration), Phys. Rev. Lett. **116** (2016).  
[11] B. P. Abbott *et al.* (LIGO Scientific Collaboration, Virgo Collaboration), Phys. Rev. Lett. **116** (2016).  
[12] B. P. Abbott *et al.* (LIGO Scientific Collaboration, Virgo Collaboration) (LIGO Scientific Collaboration and Virgo Collaboration), Phys. Rev. Lett. **119**, 141101 (2017).  
[13] B. P. Abbott *et al.* (LIGO Scientific Collaboration, Virgo Collaboration), Phys. Rev. Lett. **116** (2016).  
[14] B. P. Abbott *et al.* (LIGO Scientific Collaboration, Virgo Collaboration), Annalen Phys. **529** (2017).  
[15] B. P. Abbott *et al.* (LIGO Scientific Collaboration, Virgo Collaboration), Phys. Rev. Lett. **116** (2016).  
[16] S. E. Caudill, *Search for Gravitational Wave Bursts from Perturbed Black Holes*, Ph.D. thesis, Louisiana State University (2012).  
[17] S. Caudill, S. E. Field, C. R. Galley, F. Herrmann, and M. Tiglio, Class. Quantum Grav. **29** (2012).  
[18] J. Meidam, M. Agathos, C. Van Den Broeck, J. Veitch, and B. Sathyaprakash, Physical Review D **90** (2014).  
[19] E. Berti, V. Cardoso, and C. M. Will, Phys. Rev. D **73** (2006).  
[20] S. Dain, C. O. Lousto, and Y. Zlochower, Phys. Rev. D **78**, 024039 (2008).  
[21] H. Yang, K. Yagi, J. Blackman, L. Lehner, V. Paschalidis, F. Pretorius, and N. Yunes, PRL **118** (2017).  
[22] E. W. Leaver, Proceedings of the Royal Society of London, A. Mathematical and Physical Sciences, **402** (1985).  
[23] J. Veitch, V. Raymond, B. Farr, W. M. Farr, P. Graff, S. Vitale, B. Aylott, K. Blackburn, N. Christensen, M. Coughlin, W. D. Pozzo, F. Feroz, J. Gair, C.-J. Haster, V. Kalogera, T. Littenberg, I. Mandel, R. O’Shaughnessy, M. Pitkin, C. Rodriguez, C. Röver, T. Sidery, R. Smith, M. V. D. Sluys, A. Vecchio, W. Vousden, and L. Wade, Phys. Rev. D **91** (2015).  
[24] <http://www.black-holes.org/waveforms>.  
[25] A. H. Mroue and H. P. Pfeiffer, arXiv (2012).  
[26] A. H. Mroue *et al.*, Phys. Rev. Lett. **111**, 241104 (2013), arXiv:1304.6077 [gr-qc].  
[27] L. T. Buchman, H. P. Pfeiffer, M. A. Scheel, and B. Szilagyi, Phys. Rev. **D86**, 084033 (2012), arXiv:1206.3015 [gr-qc].  
[28] G. Lovelace, M. Scheel, and B. Szilagyi, Phys. Rev. **D83**, 024010 (2011), arXiv:1010.2777 [gr-qc].  
[29] G. Lovelace, M. Boyle, M. A. Scheel, and B. Szilagyi, Class. Quantum Grav. **29**, 045003 (2012), arXiv:1110.2229 [gr-qc].  
[30] I. Kamaretsos, M. Hannam, S. Husa, and B. S. Sathyaprakash, Phys. Rev. D **85**, 024018 (2012).  
[31] F. Echeverria, Phys. Rev. D **40**, 3194 (1989).  
[32] A. Taracchini, A. Buonanno, Y. Pan, T. Hinderer, M. Boyle, D. A. Hemberger, L. E. Kidder, G. Lovelace, A. H. Mroue, H. P. Pfeiffer, M. A. Scheel, B. Szilagyi, N. W. Taylor, and A. Zenginoglu, Phys. Rev. D **89** (2014).  
[33] D. V. Martynov *et al.*, Phys. Rev. D **93** (2016).  
[34] X. Jiménez-Forteza, D. Keitel, S. Husa, M. Hannam, S. Khan, and M. Pürrer, Phys. Rev. D **95** (2017).  
[35] P. W. H. and S. A. Teukolsky, Astrophysic J. **185**, 635 (1973).  
[36] S. Detweiler, Astrophysical Journal, Part 1 **239** (1980).  
[37] Bernard F. Schutz and Clifford, The Astrophysical Journal **291** (1985).

- [38] A. O. S. Emanuele Berti, Vitor Cardoso, *Class. Quant. Grav.* **26**, 163001 (2009).